Hindawi
Advances in Civil Engineering
Volume 2021, Article ID 2244202, 15 pages
https://doi.org/10.1155/2021/2244202

Research Article

Finite Element Model-Based Weight-Over Process Philosophy for Bridge Loading Capacity Evaluation and Rating Factor Estimation

Ali Karimpour[1,2], **Salam Rahmatalla**[1,2] **and Hossein Bolboli Ghadikolaee**[3]

[1]*Department of Civil and Environmental Engineering, The University of Iowa, Iowa City, IA 52242, USA*
[2]*Iowa Technology Institute, The University of Iowa, Iowa City, IA 52242, USA*
[3]*Hydraulic Structures, Shahid Chamran University of Ahvaz, Ahvaz, Iran*

Correspondence should be addressed to Salam Rahmatalla; salam-rahmatalla@uiowa.edu

Received 13 August 2021; Revised 6 November 2021; Accepted 24 November 2021; Published 17 December 2021

Academic Editor: Wonseok Chung

Existing rating methods estimate bridge loading capacity and demand from secondary actions due to live loads in the primary structural components. In these methods, uniaxial yielding stress is traditionally used to detect component capacity using either stress quantities or shear-moment actions to compute the capacity demand of the bridge. These approximations can lead to uncertainties in load capacity estimation. This article presents the weight-over process (WOP), a novel computer-aided approach to bridge loading capacity evaluation based on tonnage and rating factor estimation. WOP is expected to capture different forms of failure in a more general manner than existing methods. In WOP, a bridge finite element model (FEM) is discretized into many sections and element sets, each containing a single material type, and each assigned a suitable 3D failure criterion. Then, factored gross vehicle weights (GVWs) are incrementally imposed on the bridge FEM with those predefined ultimate unfavored loading scenarios in a manner similar to proof load testing. WOP code runs nonlinear analysis at each increment until a stopping criterion is met. Two representative bridges were selected to confirm WOP's feasibility and efficacy. The results showed that WOP-predicted values at the interior girders were between those of the conventional AASHTO and the nondestructive testing (NDT) strain measurement methods. That may put WOP in a favorable zone as a new method that is less conservative than AASHTO but more conservative than real NDT testing.

1. Introduction

Highway bridges are vital infrastructure that must be evaluated periodically to ensure their safe operation under traffic loading. Over their lifetime, bridges age, deteriorate, and sustain damage, ultimately becoming structurally deficient. The load-carrying capacity index is a comprehensive integrity assessment tool that engineers can use for bridge rating. The service live load that can be safely carried over a bridge is called the load rating (LR) and is expressed as a rating factor (RF). For a consistent index of load-carrying capacity, all bridges are rated by a standard set of heavy trucks or vehicular live loads (LLs). In the USA, the LR must be biennially executed based on American Association of State Highway Transportation Officials guidelines [1] and Federal Highway Administration rules [2]. The load and resistance factor rating (LRFR) method provides the RF formula for new and existing bridges as the ratio of specific LL resistance to design LL, including its dynamic effects and associated uncertainties. The RF quantity can be interpreted as the number of a particular LL that can safely cross the bridge.

There are three conventional approaches to practical LR: AASHTO analytical LR, experimental LR through either diagnosis load testing (LT) or proof LT, and finite element model- (FEM-) based LR. AASHTO LR is based on a simplified one-dimensional (1D) beam-line analysis and its prescribed provisions to rate for shear and moment separately as indicated in AASHTO's *Manual for Bridge Evaluation* [3, 4]. The experimental approach to LR uses either diagnosis LT to confirm the AASHTO analytical assumptions or proof LT to prove a bridge's capability to carry its full dead load plus some magnified LL based on in situ LT [5–8]. The third conventional approach to LR is an

advanced, reliable, and nondestructive testing (NDT) method that uses a validated bridge FEM constructed through structural model updating techniques.

The common FEM-based LR can computationally facilitate the rating process in which it transforms the bridge superstructure to several equivalent 1D composite beams in the background, similar to the conventional AASHTO LRFR method [9–12]. FEM-based LR is much more demanding than the common AASHTO method since it properly simulates 3D loading distribution inside composite members of reinforced concrete slabs as well as steel girders, consequently impacting the bridge loading capacity evaluation (BLCE) process [13]. FEM is also capable of considering the reserve capacity of the structure model up to 120 and 185% for simply supported and continuous bridges, respectively [14]. Conventionally, FEM-based LR through the allowable stress design estimates RF by comparing the allowable stress levels at different composite critical sections to those spots' values when a unique moving LL passes through a traffic lane. Then, the factored allowable stress of material and stress due to the moving LL are compared to calculate RF. FEM-based LR through LRFR calculates the ultimate capacity when the steel girder and the reinforced concrete section above it reaches a complete plastic section (PS) in which all 1D stresses are equal to the yielding points. The FEM stress levels at critical locations are automatically integrated over the composite girder cross-section as well as the effective tributary deck width to estimate maximum demands during LL traveling on a bridge model for LR [15, 16]. Although there are other ways to impose LL for BLCE and RF estimation, mostly based on analyst preference [17], both approaches deploy the uniaxial yielding criteria of each steel girder when it reaches the yielding points [11].

This article proposes a novel algorithm called the weight-over process (WOP) to rate bridge structures based on a calibrated FEM. Instead of evaluating the capacity and demand of the bridge composite girder in terms of either internal stress levels or internal actions (moments and shear forces) due to LL, WOP uses direct gross vehicle weight (GVW) to estimate capacity and demand. Since WOP considers tonnage instead of a secondary mechanism, it is expected to capture various failure mechanisms more realistically than transferring LL to associated secondary actions. First, the bridge 3D FEM is simulated and segmented into many slices. Each FEM slice resides in a spatial station along the bridge span axis, and then each slice is discretized with many element sets. WOP is programmed so that all elements that attain a single material property reside in a single element set. Second, suitable 3D failure criteria based on material type are assigned to those sets to detect the bridge's ultimate capacity. Third, WOP directly imposes LL on a bridge FEM with several prescribed loading patterns called the ultimate unfavored loading scenarios (UULSs). Finally, nonlinear analysis is performed while each UULS is incrementally imposed on each traffic lane until a PS is initiated. This process goes over all UULSs for all traffic lanes step by step, and the minimum RF for each girder is declared as its actual RF.

2. Materials and Methods

This section presents the conventional AASHTO RF philosophy and essential materials for calculating RF under different loading conditions. It then introduces the proposed WOP to estimate RF based on GVW.

2.1. AASHTO Rating Factor Method. Three AASHTO design philosophies—allowable stress rating (ASR), load factor rating (LFR), and LRFR—have been developed over recent decades. Regardless of the type of design philosophy, the RF of a bridge component can be evaluated according to AASHTO's *Manual for Bridge Evaluation* [4] as follows:

$$RF = \frac{C - (\gamma_{DC})(DC) - (\gamma_{DW})(DW) \pm (\gamma_P)(P)}{(\gamma_{LL})LL(1 + IM)}, \quad (1)$$

where C is the capacity, DC is the dead load effect, DW is the wearing surface effect, P is the permanent load, LL is the live load, and IM is the dynamic load allowance. The load factors γ_{DC}, γ_{DW}, γ_P, and γ_{LL} represent dead load factor, wearing surface load factor, permanent load factor, and LL factor, respectively. All prescribed load and resistance factors can be found in the AASHTO code. For an inventory level with a high reliability index ($\beta = 3.5$), the LL coefficient is $\gamma_{LL} = 1.75$, and for an operating level with a lower reliability index ($\beta = 2.5$), $\gamma_{LL} = 1.35$. The dead load factor is $\gamma_{DC} = 1.25$, and the wearing surface load factor is $\gamma_{DW} = 1.50$ for the strength limit state criteria. The capacity C for strength limit state can be estimated as

$$C = \phi_c \phi_s \phi R_n, \quad (2)$$

$$\phi_c \phi_s \geq 0.85, \quad (3)$$

where ϕ_c, ϕ_s, ϕ, and R_n are the condition factor, system factor, resistance factor, and nominal member resistance specified by the LRFD code, respectively [1]. The condition factor ϕ_c provides a reduction in strength due to the uncertainty in member resistance ranging from 0.85 to 1.00. The system factor ϕ_s and LRFD resistance factor ϕ are specified by code based on their limit states. Last but not least, the critical parameter in the RF formula is the dynamic allowance factor (IM). The IM indicates how much inertia could escalate the responses of the bridge model to truck-induced vibrations. The dynamic amplification factor (DAF) due to the LL speed on the bridge model can be expressed in terms of IM as follows:

$$\text{DAF} = \frac{S_{\text{dyn}} - S_{sta}}{S_{\text{sta}}} = 1 + IM, \quad (4)$$

where S_{dyn} is the peak value of the dynamic structural response and S_{sta} is the static structural response caused by the same action(s) or under the same load combination situation, estimated based on the most crucial of the understudied bridge points. AASHTO prescribes using HL-93 design truck loading for IM estimation only. The AASHTO formula for IM is [1]

$$IM = 0.33\left(1.0 - 0.125D_E\right) \geq 0, \quad (5)$$

where D_E is the minimum depth of Earth cover above the structure (ft). The IM value is estimated based on bridge surface conditions as follows: 11% for fine, smooth asphalt; 22% for intermediate clearness; and 33% at most for a very bad surface. AASHTO suggests using $IM = 0.33$ to attain high reliability when no in situ experimental testing or numerical modeling is performed. While some have reported that IM values might be much higher than the AASHTO-prescribed ones, up to $IM = 2.80$, it depends on bridge type, structural geometry, road surface condition, and truck speed [18]. Engineering judgment and in situ testing using suitable design codes can help analysts pick a fair IM value, either from guidelines or from experimental setup during RF estimation [19]. The RF obtained by (1) can be utilized to estimate the total ultimate safe weight capacity (RT) of the bridge in tonnage based on the AASHTO [4] formula (6A.4.4.4-1) as follows:

$$RT = RF \times \mathrm{GVW}, \quad (6)$$

where GVW is the gross vehicle weight of the rating truck, or LL, weight. The essential parameters to estimate RF through (1) are the capacity and demand of individual bridge composite girders under LL that must be estimated with acceptable accuracy. AASHTO code implicitly rates bridge superstructures on a component basis, meaning that a superstructure is broken down into several composite girders and each is rated independently based on its associated tributary slab width [14]. Those capacity and demand terms are expressed as internal stress values in the ASR code or internal actions as shear and moment forces in the LFR and LRFR codes; their implementations are thoroughly described in the AASHTO code.

2.2. Weight-Over Process Method. This section introduces WOP as a novel FEM-based LR method. The concept of WOP is to substitute the capacity and demand of a bridge (1) in terms of vehicular tonnage rather than secondary actions (stress, shear, moment).

2.2.1. Stage (1): Construct Calibrated FEM. The first step is to construct a detailed FEM of the bridge that comprises all primary structural components and then calibrate it through structural model updating techniques. Abaqus® was used to simulate the FEM of both bridge samples presented in this work and perform nonlinear static WOP [20]. The concrete damage plasticity model was used to detect both compressive crushing and tensile cracking at all concrete regions [21–23]. The steel material stress-strain behavior was modeled by the nonlinear curve based on Rasmussen's proposed relationship, which is superior to the conventional Ramberg-Osgood model [24]. Four steel alloys of 316L, Grade-30, Grade-42, and Grade-50 were used by the FEM, and their characteristics were chosen from the American Society for Testing and Materials (ASTM) A570 standards [25, 26]. Full composite action between the concrete slab and girders was imposed by a surface-to-surface contact algorithm, while the multipoint constraint algorithm was used to connect bridge components. In both samples' FEMs, the concrete body was modeled with a 3D 8-node iso-parametric element (C3D8R) capable of modeling plastic deformation. The reinforcement rebars were modeled as a 3D wire truss element member (T3D2) plus embedded-region constraints inside the concrete medium. The embedded-region constraint can satisfy a perfect bond between the concrete medium and reinforcement members to accurately simulate a unified reinforcement concrete object. The steel cross beams and girders were modeled with eight nodal points, six degrees of freedom, and a reduced integration shell element (S8R).

The Surface-Based Contact element type along with transverse nonlinear springs (defined by the Abaqus Connector Sections option) was used to better simulate the boundary conditions (bearing systems) along both the gravitational and transverse directions [27, 28]. The surface-based interactive elements with both normal behavior ("hard contact") and tangential behavior (penalty method) were defined to express the gravitational interaction of the superstructure over the substructure. The mesh sensitivity analysis was carried out to obtain an acceptable mesh size in which all initial 25 natural frequencies varied by less than 1%. It is required to activate geometric, boundary condition, and material nonlinearities during FEM implementations for BLCE and the LR process. The overall 3D FEM of the first bridge was simulated by 82318 nodes, while the second sample attained 375522 nodes.

After simulating the initial bridge FEM based on the as-built blueprint, it is required to perform structural model updating to validate it; model updating techniques are used to make a fair representative of the real bridge from its in situ information [29–32]. For bridge structures, the most important parameters that must be updated are boundary conditions and material properties using many available advanced techniques [33–36]. Nonlinear material models must be incorporated to develop WOP, so it can capture the yielding of the bridge in the plastic region. Material nonlinearity, geometric nonlinearity, and large displacement effects must be activated to make the FEM a more realistic representative.

2.2.2. Stage (2): Lane-Wise Segmentation and 3D Failure Criteria. The second stage of WOP is divided into two major substages. First, the FEM of the bridge superstructure is segmented and meshed such that all primary structural components attain the same mesh size along the bridge span axis. For instance, in the case of a reinforced concrete slab and steel girders system, the FEM must be meshed with the same elemental length for rebars, concrete slab, and girders. This step is essential to better capture the yielding occurrence of the composite girder for the LR process. Therefore, the FEM of each composite girder is equally segmented along its span length (e.g., X-direction) into several composite sections (N_s), and each section contains reinforced concrete elements and girder elements as shown in Figure 1.

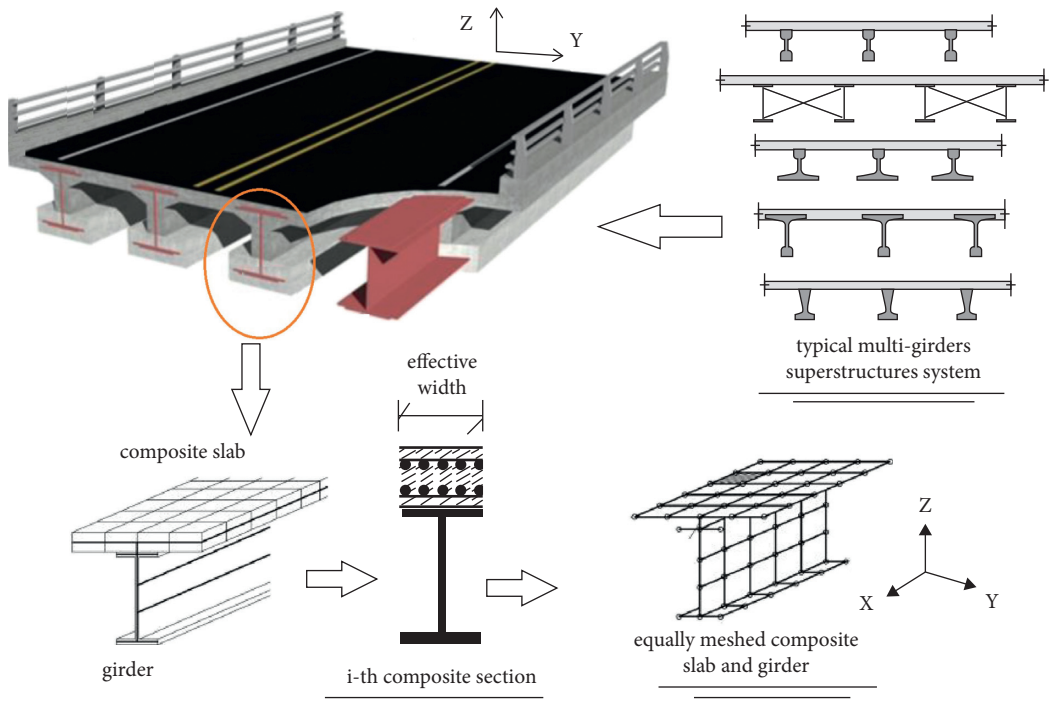

Figure 1: Girder composite section segmentation process to identify complete plastic section based on 3D failure criteria under various prescribed UULSs.

In each section, several types of bridge materials (N_m) are attributed to the concrete, rebar, and girder elements. Hence, there are ($N_s * N_m$) element sets for each composite girder of the bridge FEM; each set attains spatial characteristics to identify the sets that reside at the same section but contain different material types. Eventually, ($N_s * N_m * N_G$) FEM element sets are created by WOP for all bridge composite girders; (N_G) is the number of bridge girders.

In the second substage, appropriate 3D failure criteria are assigned to each element set based on their material types. While the bridge span is being loaded based on the WOP algorithm, some elements at several sets start to pass their yielding points. However, the plastic capacity of a composite girder is reached when all fibers inside a section pass their yielding points and enter the plastic region, and a PS is initiated based on AASHTO's *Manual for Bridge Evaluation* [4]. Since WOP deals with the 3D FEM of a composite bridge with various materials, appropriate 3D failure criteria must be chosen rather than the conventional uniaxial stress-strain relationship for LR. In general, any suitable failure criteria can be deployed to execute WOP based on material types and engineering judgment [37, 38]. Common failure surfaces for ductile and brittle materials are shown in Figure 2, in which 3D FEM stress fields can be compared to their associated uniaxial behaviors to detect PSs, since WOP automatically computes all structural components' interactions (axial-shear-flexural) and compares appropriate equivalent stress to material yield stress. In this study, the Von Mises yield criteria are used to capture the 3D yielding of FEM elements of steel components. For resilient and flexible components made with metallic materials, the Von Mises stress, or equivalent stress (σ_e), is commonly used as the failure criteria [39]:

$$\sigma_e = \sqrt{\frac{1}{2}\left((\sigma_1 - \sigma_2)^2 + (\sigma_1 - \sigma_3)^2 + (\sigma_3 - \sigma_2)^2\right)} = \sigma_y, \quad (7)$$

where σ_1, σ_2, σ_3, and σ_y are the first, second, and third principal stresses and the uniaxial yield stress, respectively, and $\sigma_1 \geq \sigma_2 \geq \sigma_3$. For structural components that are made with brittle materials such as concrete, the maximum principal stress (σ_{mps}) is used as the failure criteria hereafter. The maximum principal stress criteria state that yield occurs when the largest principal stress exceeds its correspondent uniaxial yield strength; it is expressed as [40, 41]

$$\sigma_{\text{mps}} = \begin{cases} \sigma_1 \geq \sigma_{yc}, \\ \text{OR}, \\ |\sigma_3| \geq |\sigma_{yt}|, \end{cases} \quad (8)$$

where σ_{yc} and σ_{yt} are compressive strength and tensile strength, respectively. This means that the ultimate model capacity is when, at specific FEM section (s), all concrete element sets pass σ_{mps} and all steel element sets pass σ_e, as defined in equations (7) and (8), respectively. At this point, the PSs are initiated, and, consequently, the capacity can be calculated.

2.2.3. Stage (3): Ultimate Unfavored Loading Scenarios and Imposing LLs. In the third stage, several UULSs are prescribed and then imposed sequentially on the bridge FEM to run a nonlinear analysis. The term UULS embodies the failure mechanism that could occur if an ultimate number of LL trucks is placed on the bridge at the most unfavored locations, which produce the highest internal stresses. It is

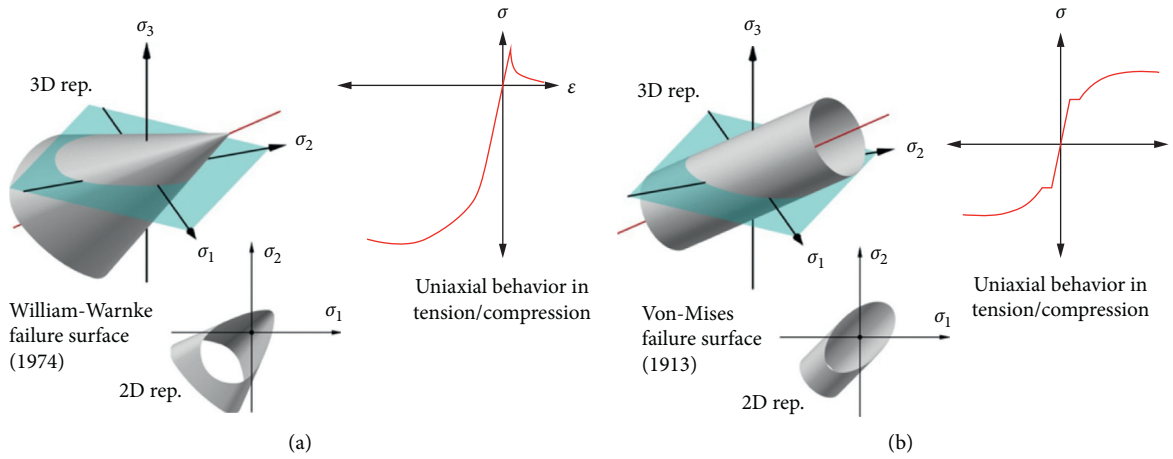

FIGURE 2: Material models in uniaxial and correspondent failure criteria: (a) concrete uniaxial stress-strain curves as its failure surface; (b) steel uniaxial stress-strain curve and its failure surface.

expected that UULS will generate worst-case loading scenarios to quickly initiate yielding on the bridge. For each UULS, all traffic lines are iteratively loaded by LL until a plastic section is initiated as an indication of the ultimate loading capacity of the bridge. Whether the bridge is simply supported or continuous span, several UULSs (N_u) can be imposed on the bridge's FEM to generate the worst loading patterns in the primary structural components. For shear failure, the most unfavorable position is close to the bridge support, and for flexural maximum action, it is the bridge midspan [7, 14, 15, 42]. There are three UULSs $(N_u = 3)$ for a single-span simply supported bridge, as shown in Figure 3. The order in which LLs are imposed on the bridge is indicated by the numbers on the trucks in Figure 3. UULS-1 activates the flexural failure by imposing an LL from the midspan toward the bridge sides, while UULS-2 and UULS-3 activate the shear failure by imposing LLs from the sides toward the midspan.

The number of traffic lanes on bridges can be determined by $(W/3600)$ in millimeters, which divides the clear roadway width (W) curbs to a standard lane width [1]. At each traffic lane, an integer number of LL, called the geometric number (N_g), can be placed practically and is defined as follows:

$$N_g = \text{floor}\left(\frac{L_{BL}}{L_{LL}}\right), \tag{9}$$

where L_{BL}, L_{LL}, and "floor" represent the bridge span length, LL vehicle length, and floor function, which rounds the "N_g" value to the closest and smallest integer number. Since in the proof LT an integer number of LL can be imposed on a bridge and WOP replicates the proof LT numerically, "N_g" must be an integer and not a decimal in order to accurately represent proof LT scenarios. This geometric number indicates how many LL can be practically imposed on FEM to replicate realistic loading conditions. In order to be conservative when imposing the legal load, it was assumed that the trucks were placed on each lane, bumper to bumper, without any spacing between them, similar to what happens during proof load testing. The way LL is imposed on FEM, illustrated in equation (10), is to artificially replicate proof LT in a numerical setup. For any bridge type, (N_u) numbers of UULSs exist. In each case, the order of imposing LLs is specified by a number associated with UULS-i, as shown in Figures 3–5. At each analysis step, one LL (GVW_i) is magnified by AASHTO factors and then added to the FEM at the ith spot, which is specified in UULS. For the ith UULS, the overall sequential loading pattern is implemented as follows:

$$W(i) = \sum_{\text{step}=1}^{N_g} \left[\gamma_{LL}(\text{GVW}_i * \text{step})(1 + IM)\right] + \begin{cases} 0 & \text{step} \le N_g \\ W_{\text{lane}} & \text{step} > N_g \end{cases}, \tag{10}$$

where GVW_i and W_{lane} are the GVW imposed by the ith UULS order and incremental lane weight loading, respectively. $W(i)$ is the weight of LL on the bridge FEM during imposing the ith UULS. In the first loading phase, each traffic lane is loaded from one LL up to N_g number of LL with a specified order defined by the ith UULS. In the second loading phase, W_{lane}, which represents artificial uniform LL, is increased from zero to infinity until the failure criteria at PS(s) are initiated and declared. The LL was multiplied by appropriate AASHTO load factors and the dynamic factor to be consistent with equation (1). At each analysis step, if PS is initiated, WOP stops, and critical weight is reported for the ith UULS and associated traffic lane. This allows the critical weights to be identified with respect to the bridge geometrics constraints. Equation (10) could be considered the numerical proof LT implementation on the bridge FEM as well. To impose LLs on a bridge FEM, WOP uses loading patterns; the vehicular tire contact patch areas are loaded with their associated GVW and axle configuration. The only LL truck model used in this article is AASHTO HL-93, but any other LL can be used by adjusting the axle configurations. The HL-93 truck comprises three axles with a total GVW of $W_{LL} = 325\,(KN)$, an overall vehicle length of $L_{LL} = 8.6 \sim 13.3\,(m)$, and a truck loading width of $L_{lr} = 1.8\,(m)$, as shown in

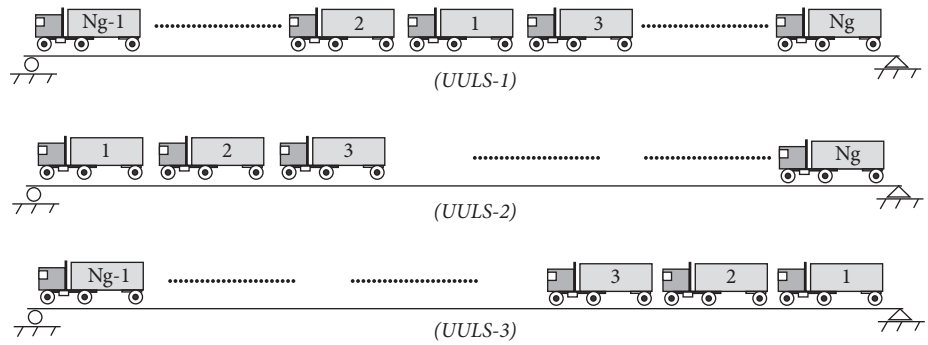

Figure 3: The UULS prescribed by WOP for a single-span simply supported bridge.

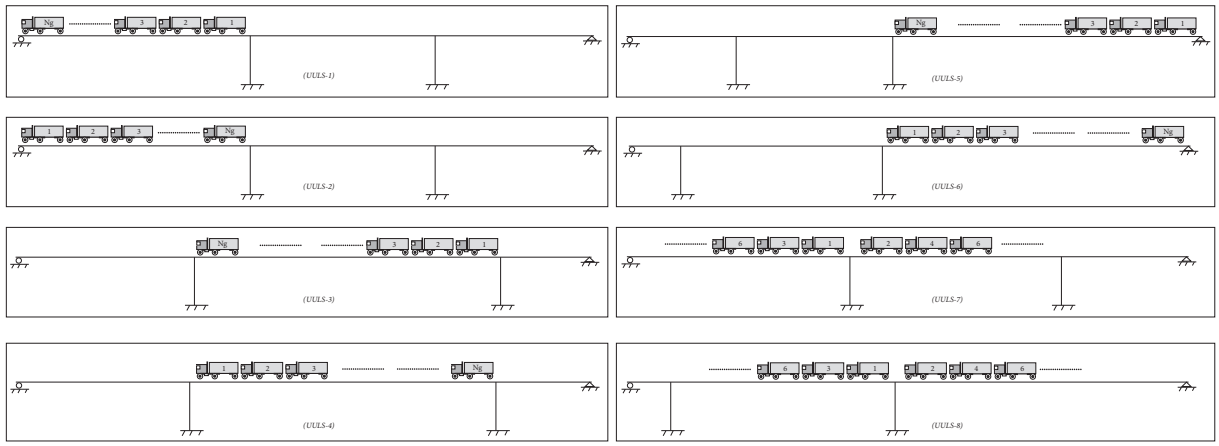

Figure 4: The UULS for shear modes prescribed by WOP for the three-span continuous bridge.

Figure 6. A tire contact patch area of 250 mm × 510 mm and a transverse distance of 1.8 m are used to select affected FEM nodes, supposing that each truck centreline coincides with the traffic lane centreline.

2.2.4. Stage (4): Quantify BLCE. Equation (1) requires that bridge capacity be deducted by the associated resistance factors indicated in equation (2). To meet this criterion, FEM materials can be manipulated through WOP. The stress-strain $(\sigma - \varepsilon)$ datasets are adjusted to the reduced stress levels by resistance factors $(\phi_c \phi_s \phi)$ as follows:

$$(\sigma, \varepsilon) \longrightarrow \left(\left[\phi_c \phi_s \phi \times \sigma\right], \varepsilon\right). \tag{11}$$

Also, to estimate the remained capacity of the bridge in the equation (1) numerator, the dead loads, wearing surface loads, and permanent loads $(\gamma_{DC}(DC) + \gamma_{DW}(DW) \pm \gamma_P(P))$ are also enlarged, based on prescribed AASHTO load factors, and then imposed on the bridge FEM. The following steps will be taken to implement $W(i)$ on the FEM. As described in stage (3), there are (N_u) numbers of UULSs, depending on whether the bridge is single-span simply supported or continuous span. From each UULS, one critical weight $W_{cr}(i)$ can be estimated by summing all loaded FEM nodal forces of "m" nodes, which are located at "n" pivotal lanes (F_m^n) at the moment of PS initiation as follows:

$$W_{cr}(i) = \sum_{n=1}^{N_t^i} \left[\sum_{m=1}^{N_t^i} F_m^n \right]; \quad i = 1{:}\ N_u, \tag{12}$$

where N_t^i and N_n^i are the number of loaded traffic lanes and the number of loaded FEM nodes for the ith UULS, respectively. From those (N_u) cases, the primary critical weight (W_{cr}^P) is the minimum weight at which the bridge collapses, as follows:

$$W_{cr}^P = \min\{W_{cr}(i)\}; \quad i = 1{:}\ N_u. \tag{13}$$

So far, the remained capacity of the bridge in weight/tonnage quantity has been estimated by (W_{cr}^P), while appropriate AASHTO factors were inserted during WOP implementation to be consistent with the numerator of equation (1). As indicated in equation (1), the vehicular LL capacity and demand are stress quantity in the ASR method or shear-moment actions in the LFR and LRFR methods. In order to attain unit consistency, the demand of vehicular LL in the WOP method is the LL weight; thus, the LL of the denominator of equation (1) must be substituted with a single GVW that has the same unit (tonnage) as the remained capacity W_{cr}^P. Therefore, the FEM-based RF based on the proposed WOP can be evaluated as follows:

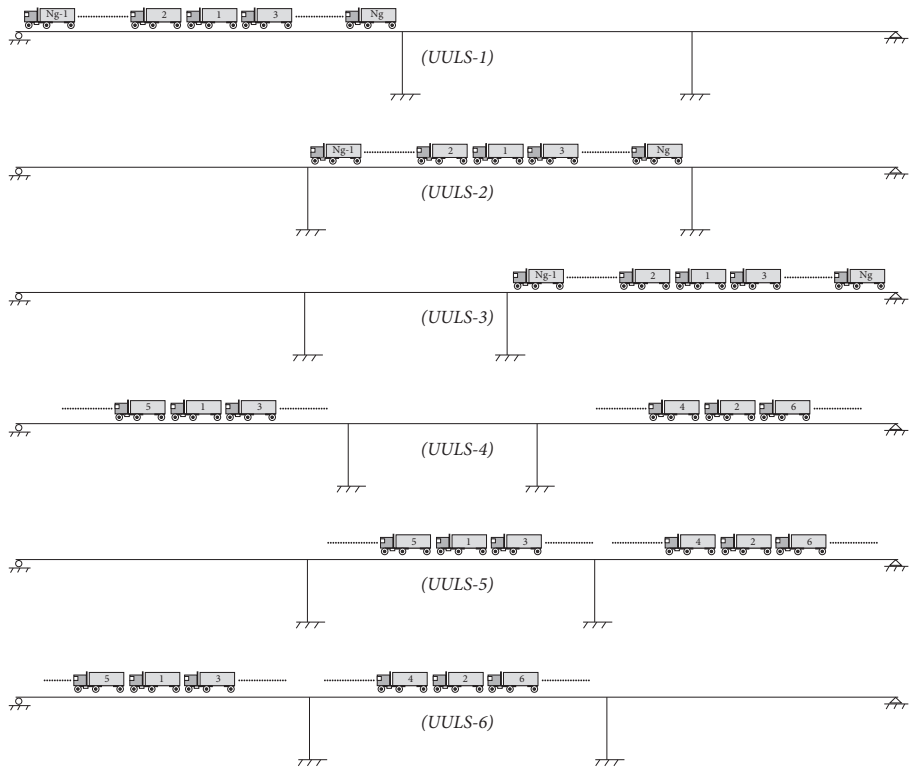

Figure 5: The UULS for flexural modes prescribed by WOP for the three-span continuous bridge.

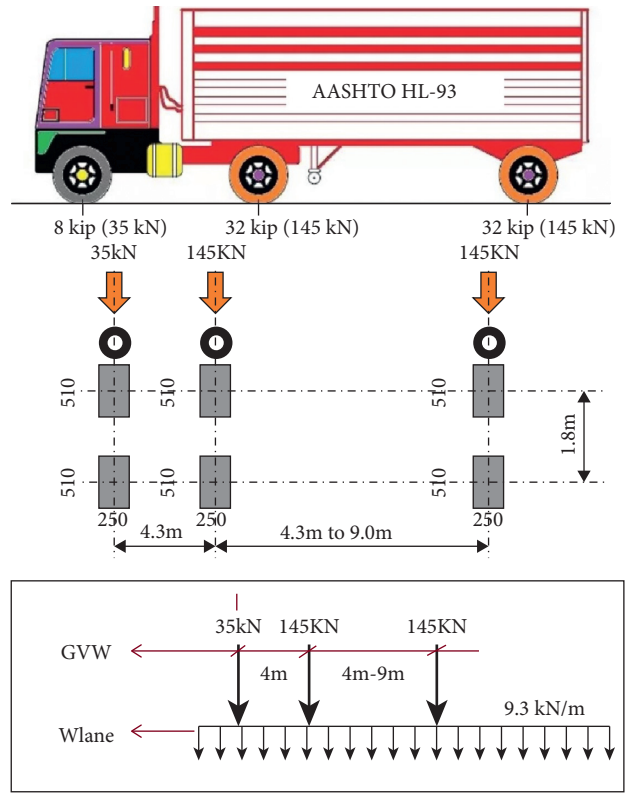

Figure 6: AASHTO design truck HL-93 and its axle configuration, tire pressure areas, GVW, and minimum lane loading.

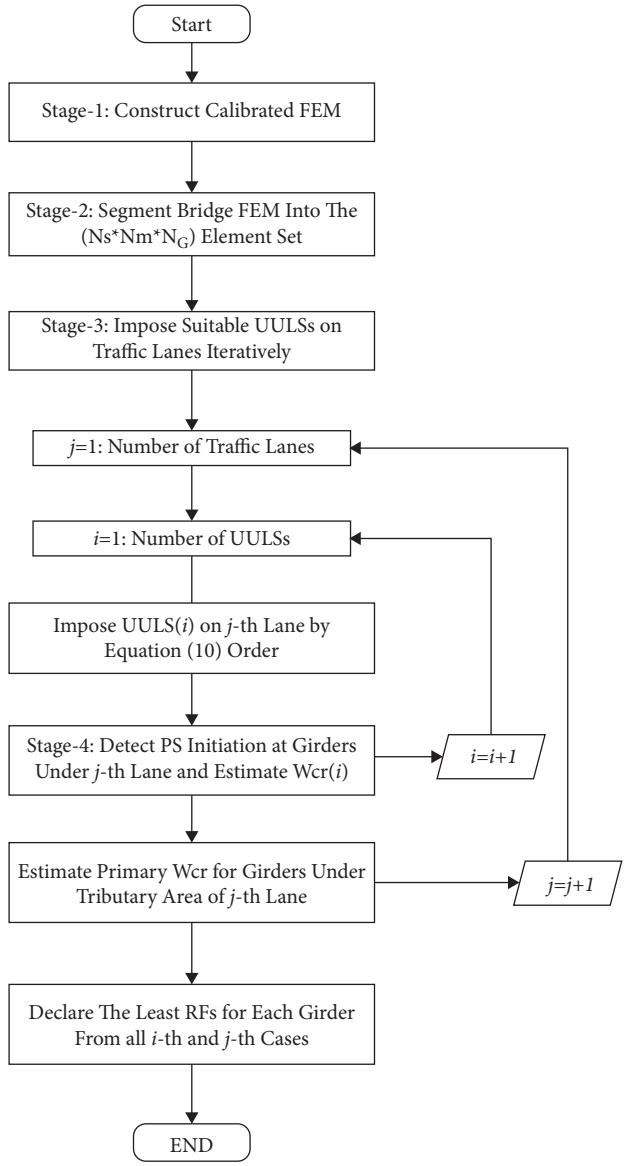

Figure 7: Flow chart of the proposed WOP deployed for BLCE, LR, and RF estimation.

$$RF = \frac{\text{bridge remained capacity}}{\text{single } LL \text{ demand}} = \frac{W_{cr}^{P}}{\gamma_{LL}\left[1 * \text{GVW}\right](1 + IM)}. \tag{14}$$

The WOP algorithm is depicted in a flowchart in Figure 7 that shows the stages one by one.

3. Numerical Implementation

3.1. First Bridge Sample. To deploy and validate the WOP for a real bridge, a sample bridge in Iowa (FHWA #31690) was selected. As-built blueprints were received from the Iowa Department of Transportation and used to construct the FEM of the bridge. It is a single-span simply supported composite bridge with a reinforced concrete deck, steel plate girders, and cross beams, as shown in Figure 8(a). The bridge has a length $L_{Bl} = 18.5\,(m)$, a span width $L_{Bw} = 9.15\,(m)$, two traffic lanes $N_{tl} = 2$, four girders ($N_G = 4$), and a geometric number $N_g = 2$. The UULS for a single-span bridge is shown in Figure 3 for the most severe load configuration and truck position. The FEM of the first sample and its traffic lane loaded by HL-93 LL are shown in Figures 8(b) and 8(c).

3.1.1. WOP Results of the First Sample. DW is mostly conferred to the layer of asphalt with a weight of 23 kN/m^3. After constructing the bridge FEM based on blueprints and material models, both traffic lanes and their affected nodes under AASHTO design load (HL-93 truck) characteristics were defined as shown in Figures 8(b) and 8(c). The baseline FEM has a concrete strength of 20 MPa, steel ST 316L, and reinforcement material with steel Grade-30. For the baseline case of the first sample, the failure mode is a flexural mode triggered by the UULS-1 load case. The plot of the first sample's

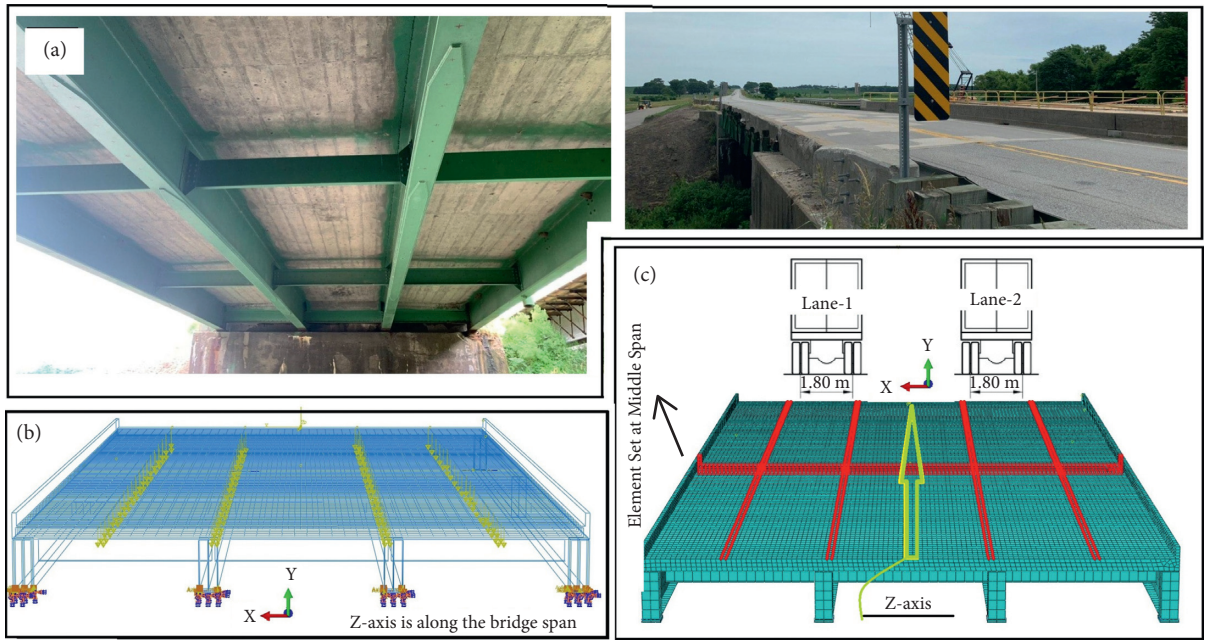

FIGURE 8: First representative bridge (FHWA #31690): (a) bridge superstructure; (b) bridge FEM with associated traffic lanes; (c) segmented bridge FEM with element sets to detect PS(s).

structural components (concrete deck, steel girder, and reinforcement network) under the first traffic lane loaded by UULS is shown in Figure 9. Due to the sample symmetry, two PSs were generated, PS1 and PS2. Although the plastic hinge theoretically happens exactly in the middle of a homogenous girder under flexural failure, the first PS occurs at stations of $0.38 * L_{Bl}$ and $0.62 * L_{Bl}$, spaced 12% from the bridge's middle station due to the composite action of the superstructure, various material yielding behaviors, and 3D modeling.

3.1.2. Sensitivity Analysis. It is common to deploy FEM in order to perform sensitivity analysis to confirm experimental results or potential outcomes of severe incidents such as damage scenarios, strengthening of components, and corrosion [43] Therefore, the four following sensitivity analysis cases are defined and analyzed to compare BLCE and RF. In Figure 10, the force displacement of the WOP nonlinear analysis is shown; the force is the total reaction force of the bridge FEM toward the midspan deflection. Figure 11 shows the estimated RFs for the various cases as well.

(1) Rebar Reduction Strength. The first adjustment in the FEM was to reduce the area of the reinforcement rebars by 50%; results are indicated in the plots by "Rebar Reduction Case." Rebar corrosion happens in reinforced concrete structures due to cover cracking, spalling, and degradation of the outer concrete layers; this causes a reduction in the rebar cross-sectional area at high levels of corrosion [43]. To investigate the rebar strength for the BLCE, only the reinforcement area properties were adjusted; all other parameters were kept constant with baseline FEM.

(2) Increasing Concrete Strength. The second case study increased the concrete strength to investigate its effects on the BLCE and RF of the bridge structures; results are indicated in the plots by "Enhanced Concrete Case." For this sensitivity study, the concrete strength for the bridge deck was enhanced from 20 MPa to 40 MPa in the FEM code to determine its effects on BLCE. It is assumed that all other structural system characteristics remained constant.

(3) Increasing Steel Girder Strength. The third case study increased the steel girder strength to investigate its effects on the BLCE and RF of bridge structures; results are indicated in the plots by "Enhanced Steel Case." For this sensitivity study, the steel strength for the bridge girders was enhanced from steel 316L to steel Grade-42 in the FEM code to determine its effects on BLCE. Again, it is assumed that all other structural system characteristics remained constant.

(4) Settlement Sensitivity Analysis. The last sensitivity study simulated settlement modeling for one of the interior girders to investigate its effects on BLCE and RF. Results are indicated in the plots by "Single Settlement Case." This is among the most prevalent damage in a bridge structure that happens immediately after construction or during its lifetime. The deflection of bridges is limited to the span length divided by 800 ($L/800$) for simple and continuous spans and $L/300$ for cantilever arms [4]. To simulate a severe settlement scenario above the allowable deflection limits, a settlement of $\delta = L_{Bl}/200 = 9.2\,(cm)$ was considered on one side of an interior girder to do a sensitivity study.

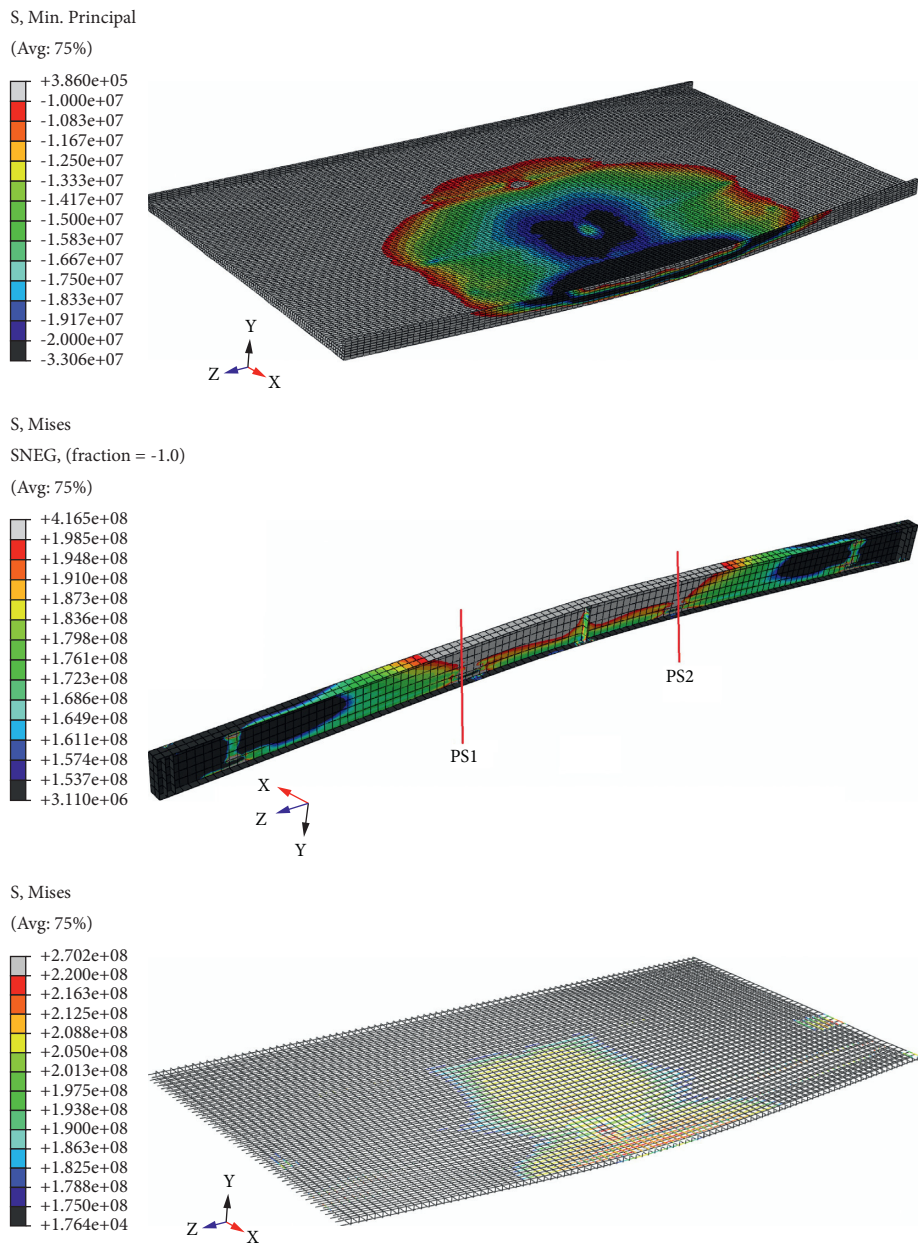

Figure 9: The bridge component stress fields at the moment of PS initiation under UULS-1 at the first traffic lane as a sample of UULS stress fields.

3.2. Second Bridge Sample. The second sample is the Powder Mill Bridge (PMB), a three-span continuous composite concrete deck with steel girders located in Massachusetts. The exterior span length is 11.75 m, the interior span is 23.5 m, there are six girders ($N_G = 6$), and the overall bridge length is 47 m, as shown in Figure 12(a). There were two main reasons for selecting PMB as the second sample. The first was to test WOP for a continuous bridge model. The second was that its information and experimental RFs are available in the literature [43–46]. In these references, the three RFs for each bridge girder are the AASHTO conventional LR approach, LR modified by NDT data, and conventional FEM-based LR. The NDT method uses field measurements to adjust and scale AASHTO-proposed distribution factors and, consequently, estimate RFs [43]. This type of NDT data is normally used to calibrate the girder distribution factor and the actual girder loading capabilities based on in situ information from strain measurements. While the NDT result is not perfect, it is considered the most trusted and authentic outcome since it illuminates as-is and real structural behavior in its operational conditions.

The FEM of the PMB was remodeled in Abaqus by this article's authors based on detailed geometric information and material strengths presented in the references (see Figure 12(b)). Fourteen UULSs were defined by the authors to impose potential severe LL positioning. The UULSs were defined from three-span continuous influence line concepts; they either generate maximum shear internal actions at girder supports (or bridge pier cap spots) or maximum

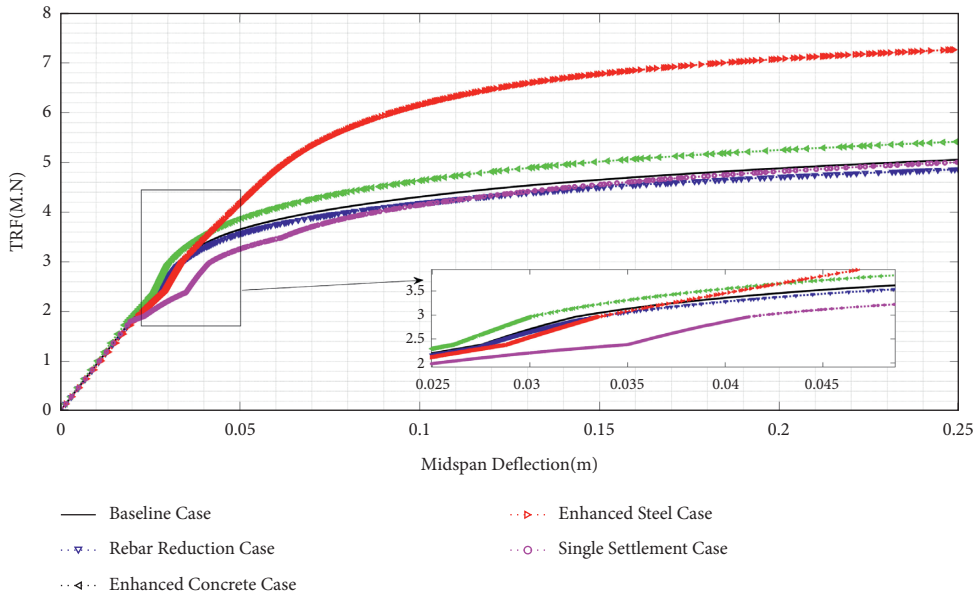

Figure 10: Force displacement curves of the first bridge specimen for the baseline case and the other four cases.

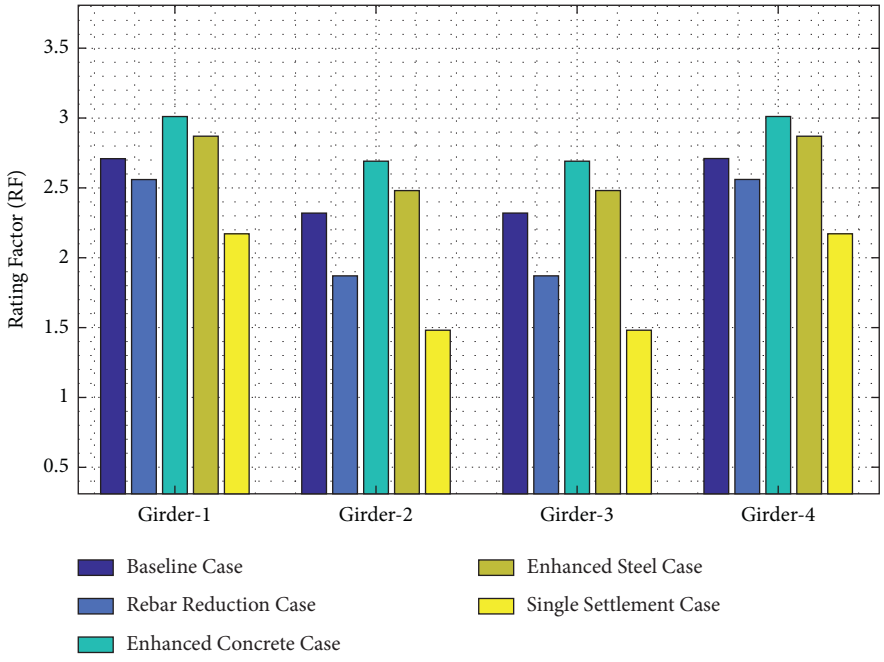

Figure 11: Rating factors of the first bridge specimen for the baseline case and the other four cases.

flexural moment at the midspan of each girder span (s). In general, the overall UULSs must contain all potential severe LL placements, which have the highest internal effects on the bridge's primary structural components. The overall UULSs are separated based on their potential failure modes: shear UULS, shown in Figure 4, and flexural UULS, shown in Figure 5. Rating factors estimated by WOP and those reported in the literature are compared in Figure 13.

3.3. Recommendation for Practical Implementation. To successfully implement the WOP for real-world bridge LR, the first and essential practical step is to perform the structural model updating process to construct a fair representation of the bridge by its FEM as explained in the WOP first stage. Although, in general, any available robust model updating technique can be exploited to perform WOP's first stage, detailed descriptions of the model

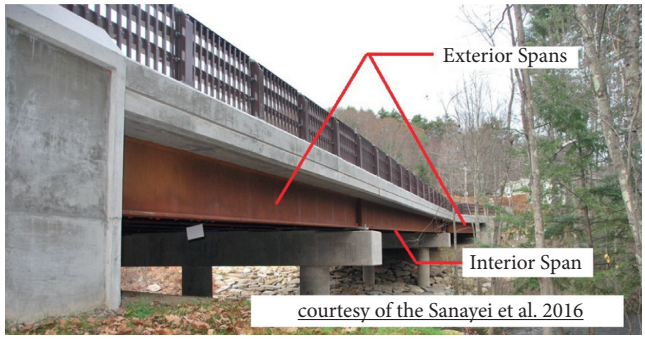

(a)

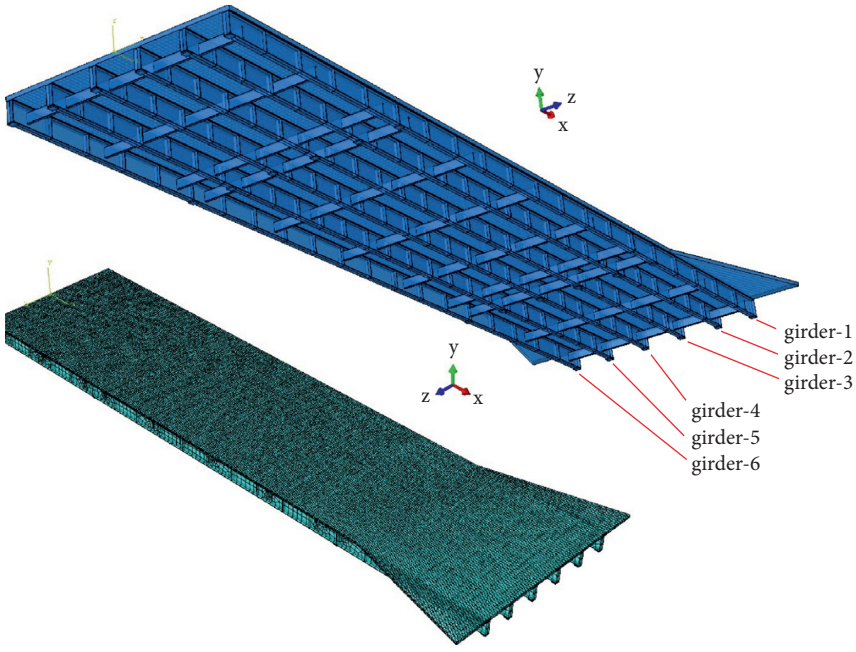

(b)

Figure 12: Second bridge specimen (PMB): (a) PMB bridge, courtesy of Sanayei et al. [43]; (b) the PMB FEM simulated by the authors in Abaqus® to execute and confirm WOP.

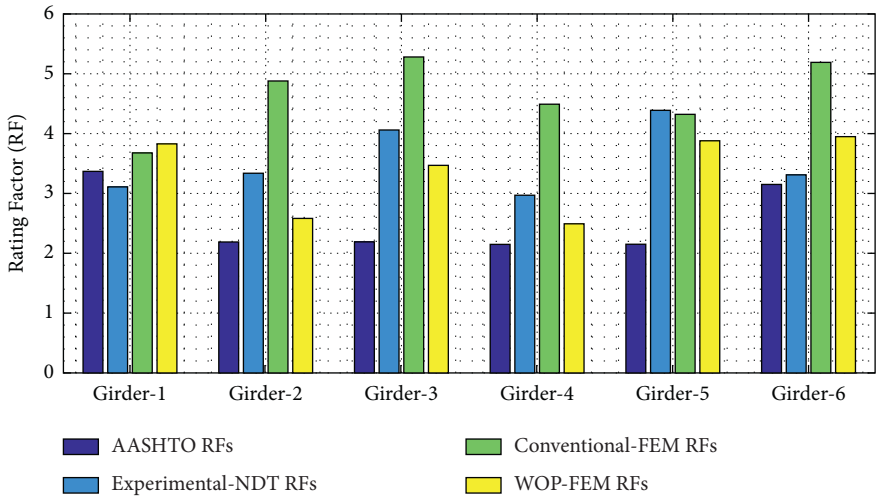

Figure 13: Comparison of WOP RFs with AASHTO, NDT, and conventional FEM LR methods as indicated in the literature [43, 44].

updating techniques used in this article are available in the references [29, 30]. After simulating the initial FEM based on the as-built blueprints of a bridge, the analyst must calibrate its FEM either with in situ NDT data or visual inspections based on AASHTO guidelines for field inspection. With the exception of the first WOP step, all other stages can be executed with the developed computer program that imposes the potential UULS and declares RFs with higher accuracy.

4. Conclusions

This article proposes a methodology called the weight-over process (WOP) to evaluate a bridge's ultimate capacity and its RFs based on actual GVW in excessive traffic scenarios. By considering rightful GVW instead of secondary action estimations, WOP could capture various failure mechanisms with higher accuracy than other conventional approaches.

The WOP process examines all traffic lanes to find the most critical RF for each girder and then declares the minimum RF for each girder to be the dominant RF. With WOP, there is no need to manually find the RF in the negative and positive sections; WOP incrementally places the LLs at the critical spots defined as UULS. Bridge failure mode in the case of excessive traffic loading is also identified through WOP and can be used for the rehabilitation plan, depending on the type of failure. It is well known that all FEM-based LR approaches return higher RFs than the AASHTO method because they consider the reserved material capacity and structural redundancies and also incorporate 3D composite action between different components accurately without any simplification.

For the first bridge sample, several sensitivity analyses were defined by changing the rebar area, concrete strength, steel girder strength, and settlement to find the most critical components in the BLCE and RFs. It was indicated that the settlement phenomenon is the most crucial cause of damage because it decreased RF tremendously relative to the other simulations. For the second bridge sample's exterior girders, WOP returns higher RFs than the experimental NDT method, while for interior girders it returns lower RFs. Except for the first girder, WOP results are much closer to the experimental NDT LR method than those of the conventional FEM-based method, as shown in Figure 13.

Except for small differences at girders 1 and 5, the results in Figure 13 show that WOP demonstrated better performance than the conventional FEM. The NDT data could be considered the best available reference for comparison and validation purposes with WOP; it compares theoretical strains with measured strains and scales the conventional AASHTO rating based on these differences [43, 46]. At the interior girders, WOP-predicted values were between those of AASHTO and NDT, which may indicate that it is less conservative than AASHTO but more conservative than the real (NDT) testing.

As shown in Figure 13, WOP returns higher RFs than the AASHTO and NDT LR methods for the exterior girders and lower RFs than the NDT LR method for the interior girders. This could be related to the nature of the NDT data used in this work. The NDT used measured strain to enhance the conventional AASHTO rating, and it seems that the external girders were not sufficiently stressed during the testing [43]. That could be why WOP presents higher values than NDT. Another issue could be the lack of information about sidewalk barriers and guardrails; their equivalent dead loads were assumed and then approximately imposed by the authors. The lower rating by WOP for the interior girders could be related to how the strain data was scaled for the NDT method or to the possibility that the 3D failure criteria and stress field could capture secondary stress fields during PS capacity estimation more effectively than the conventional 1D approaches. Except for girders 1 and 5, WOP returns were closer to the experimental RFs than those of the conventional FEM-based method. In the case of girders 1 and 5, the deviation from the real experimental RF is very small. Also, the bridge FEM in the second example was resimulated by the authors based on information provided in the references.

The main computational cost of WOP is attributed to its implementation for different types of bridges. Difficulties such as the FEM segmentation, UULS definition, and sequential analysis steps could be valid concerns for program developers. Commercial software must be reprogrammed and upgraded to automatically prescribe UULSs from its library and impose sequential LLs on the FE model. Also, an FE model segmentation stage is needed to slice the model along its pivotal axis to myriad spatial stations/elements that require swift processors in practice.

Data Availability

All the datasets and the finite element code used in this article are available via the Data On-Request option. This dataset can be obtained by contacting the first author, Dr. Ali Karimpour (ali-karimpour@uiowa.edu). The experimental dataset for the second example is also available in references [43, 46].

Disclosure

The contents reflect the views of the authors, who are responsible for the facts and the accuracy of the information presented herein and are not necessarily representative of the sponsoring agencies.

Conflicts of Interest

The authors declare that there are no conflicts of interest regarding the publication of this paper.

Acknowledgments

The first and second authors disclosed receipt of the following financial support for the research, authorship, and/or publication of this article: this work was supported by the Mid-America Transportation Center via a grant from the U.S. Department of Transportation's University Transportation Centers Program (grant number: DOT 69A3551747107), which is gratefully acknowledged.

References

[1] Aashto, *AASHTO LRFD Bridge Design Specifications*, American Association of State Highway Transportation Officials, Washington, DC, USA, 2017.

[2] Fhwa, *Bridge Inspector's Reference Manual (BIRM) (FHWA-NHI-03-001/002)*, Federal Highway Administration, Washington, DC, USA, 2006.

[3] O. Russian, A. Belarbi, Q. Feng, and M. Dawood, "Investigation of material properties for load rating of historical bridges," *Journal of Bridge Engineering*, vol. 25, no. 4, Article ID 04020014, 2020.

[4] Aashto, *Manual for Bridge Evaluation*, American Association of State Highway Transportation Officials, Washington, DC, USA, 3rd edition, 2018.

[5] E. O. L. Lantsoght, "Editorial: diagnostic and proof load tests on bridges," *Frontiers in Built Environment*, vol. 6, Article ID 586704, 2020.

[6] E Lantsoght, Ed., *Load Testing of Bridges: Current Practice and Diagnostic Load Testing*, CRC Press, Leiden, Netherlands, 2019.

[7] E. Lantsoght, C. van der Veen, A. de Boer, and D. Hordijk, "Collapse test and moment capacity of the Ruytenschildt reinforced concrete slab bridge," *Structure and Infrastructure Engineering*, vol. 13, no. 9, pp. 1130–1145, 2017a.

[8] E. O. L. Lantsoght, C. van der Veen, A. de Boer, and D. A. Hordijk, "State-of-the-art on load testing of concrete bridges," *Engineering Structures*, vol. 150, pp. 231–241, 2017.

[9] V. Shahsavari, M. Mehrkash, and E. Santini-Bell, "Damage detection and decreased load-carrying capacity assessment of a vertical-lift steel truss bridge," *Journal of Performance of Constructed Facilities*, vol. 34, no. 2, Article ID 04019123, 2020.

[10] M. Aghagholizadeh and N. Catbas, "Comparative analysis and evaluation of two prestressed girder bridges," *Current Trends in Civil & Structural Engineering*, vol. 3, no. 5, 2019.

[11] Computers and Structures Inc, *CSI Analysis Reference Manual for SAP2000, ETABS®, SAFE®, and CSiBridge™*, Computers and Structures, Inc, Berkeley, CA, USA, 2019.

[12] Aashto, "AASHTOWare Bridge: design, rate, inventory, inspect, and manage," 2020, https://www.aashtoware.org.

[13] A. G. Soto, A. P. Caldentey, H. C. Peiretti, and J. C. Benítez, "Experimental behaviour of steel-concrete composite box girders subject bending, shear and torsion," *Engineering Structures*, vol. 206, Article ID 110169, 2020.

[14] A. Gheitasi and D. K. Harris, "Failure characteristics and ultimate load-carrying capacity of redundant composite steel girder bridges: case study," *Journal of Bridge Engineering*, vol. 20, no. 3, Article ID 05014012, 2015.

[15] M. J. A. Albraheemi, W. G. Davids, A. Schanck, and S. Tomlinson, "Evaluation and rating of older non-composite steel girder bridges using field live load testing and nonlinear finite element analysis," *Bridge Structures*, vol. 15, no. 1-2, pp. 27–41, 2019.

[16] F. A. Sofi and J. S. Steelman, "Nonlinear flexural distribution behavior and ultimate system capacity of skewed steel girder bridges," *Engineering Structures*, vol. 197, Article ID 109392, 2019.

[17] M. Ju, D. Moon, G. Kim, and J. Sim, "Evaluating rating factor for prestressed concrete girder bridges by nonlinear finite element analysis," *Structure and Infrastructure Engineering*, vol. 11, no. 9, pp. 1250–1262, 2015.

[18] L. Deng, C. S. Cai, and M. Barbato, "Reliability-based dynamic load allowance for capacity rating of prestressed concrete girder bridges," *Journal of Bridge Engineering*, vol. 16, no. 6, pp. 872–880, 2011.

[19] M. Nouri and S. Mohammadzadeh, "Probabilistic estimation of dynamic impact factor for masonry arch bridges using health monitoring data and new finite element method," *Structural Control and Health Monitoring*, vol. 27, no. 12, Article ID e2640, 2020.

[20] Dassault Systems Simulia Corp, *ABAQUS. Velizy-Villacoublay*, Dassault Systems Simulia Corp, France, Europe, 2017.

[21] H. Ataei and M. Mamaghani, *Finite Element Analysis: Applications and Solved Problems Using Abaqus®*, CreateSpace Independent Publishing Platform, Scotts Valley, CA, USA, 2018.

[22] M. Hanifehzadeh, B. Gencturk, and K. Willam, "Dynamic structural response of reinforced concrete dry storage casks subjected to impact considering material degradation," *Nuclear Engineering and Design*, vol. 325, pp. 192–204, 2017.

[23] D. J. Carreira and K. H. Chu, "Stress-strain relationship for reinforced concrete in tension," *ACI Journal Proceedings*, vol. 83, no. 1, pp. 21–28, 1986.

[24] K. J. R. Rasmussen, "Full-range stress-strain curves for stainless steel alloys," *Journal of Constructional Steel Research*, vol. 59, no. 1, pp. 47–61, 2003.

[25] M. Bahirai, M. Gerami, and V. Bahaari Zargar, "Postannealing mechanical properties of structural steel St37," *Journal of Materials in Civil Engineering*, vol. 32, no. 7, Article ID 04020152, 2020.

[26] R. Carreño, K. H. Lotfizadeh, J. P. Conte, and J. I. Restrepo, "Material model parameters for the Giuffrè-Menegotto-Pinto uniaxial steel stress-strain model," *Journal of Structural Engineering*, vol. 146, no. 2, Article ID 04019205, 2020.

[27] Y. Pan, A. K. Agrawal, and M. Ghosn, "Seismic fragility of continuous steel highway bridges in New York State," *Journal of Bridge Engineering*, vol. 12, no. 6, pp. 689–699, 2007.

[28] Y. Pan, A. K. Agrawal, M. Ghosn, and S. Alampalli, "Seismic fragility of multispan simply supported steel highway bridges in New York State. I: bridge modeling, parametric analysis, and retrofit design," *Journal of Bridge Engineering*, vol. 15, no. 5, pp. 448–461, 2010.

[29] A. Karimpour and S. Rahmatalla, "Identification of structural parameters and boundary conditions using a minimum number of measurement points," *Frontiers of Structural and Civil Engineering*, vol. 14, no. 6, pp. 1331–1348, 2020.

[30] A. Karimpour and S. Rahmatalla, "Extended empirical wavelet transformation: application to structural updating," *Journal of Sound and Vibration*, vol. 500, Article ID 116026, 2021.

[31] R. Lostado Lorza, R. Escribano García, R. Fernandez Martinez, and M. A. M. Calvo, "Using genetic algorithms with multi-objective optimization to adjust finite element models of welded joints," *Metals*, vol. 8, no. 4, p. 230, 2018.

[32] S. Íñiguez-Macedo, R. Lostado-Lorza, R. Escribano-García, and M. Á Martínez-Calvo, "Finite element model updating combined with multi-response optimization for hyper-elastic materials characterization," *Materials*, vol. 12, no. 7, p. 1019, 2019.

[33] R. Lostado, R. F. Martinez, and B. J. Mac Donald, "Determination of the contact stresses in double-row tapered roller bearings using the finite element method, experimental analysis and analytical models," *Journal of Mechanical Science and Technology*, vol. 29, no. 11, pp. 4645–4656, 2015.

[34] R. Lostado, F. J. Martínez-De-Pisón, A. Pernía, F. Alba, and J. Blanco, "Combining regression trees and the finite element method to define stress models of highly non-linear

mechanical systems," *The Journal of Strain Analysis for Engineering Design*, vol. 44, no. 6, pp. 491–502, 2009.

[35] R. Lostado, F. J. Martínez-de-Pisón, R. Fernández, and J. Fernández, "Using genetic algorithms to optimize the material behaviour model in finite element models of processes with cyclic loads," *The Journal of Strain Analysis for Engineering Design*, vol. 46, no. 2, pp. 143–159, 2011.

[36] R. Lostado, R. Escribano García, and R. Fernandez Martinez, "Optimization of operating conditions for a double-row tapered roller bearing," *International Journal of Mechanics and Materials in Design*, vol. 12, no. 3, pp. 353–373, 2016.

[37] X. Zhang, H. Wu, J. Li, A. Pi, and F. Huang, "A constitutive model of concrete based on Ottosen yield criterion," *International Journal of Solids and Structures*, vol. 193-194, pp. 79–89, 2020.

[38] J.-Y. Liang and Y.-M. Li, "A failure criterion considering stress angle effect," *Rock Mechanics and Rock Engineering*, vol. 52, no. 4, pp. 1257–1263, 2019.

[39] H. Altenbach and V. A. Kolupaev, "Classical and non-classical failure criteria," in *Failure and Damage Analysis of Advanced Materials*, H. Altenbach and T. Sadowski, Eds., Springer, New York, USA, 2015.

[40] E. J. Hearn, "Theories of elastic failure," *Mechanics of Materials: The Mechanics of Elastic and Plastic Deformation of Solids and Structural Materials*, Elsevier, Amsterdam, Netherlands, pp. 401–429, 1997.

[41] F. A. Leckie and D. J. D. Bello, "Failure criteria," in *Strength and Stiffness of Engineering Systems. Mechanical Engineering Series*, pp. 1–15, Springer, New York, 2009.

[42] O. Hasançebi and T. Dumlupınar, "Detailed load rating analyses of bridge populations using nonlinear finite element models and artificial neural networks," *Computers & Structures*, vol. 128, pp. 48–63, 2013.

[43] M. Sanayei, J. E. Phelps, J. D. Sipple, E. S. Bell, and B. R. Brenner, "Instrumentation, nondestructive testing, and finite-element model updating for bridge evaluation using strain measurements," *Journal of Bridge Engineering*, vol. 17, no. 1, pp. 130–138, 2012.

[44] E. S. Bell, P. J. Lefebvre, M. Sanayei, B. Brenner, J. D. Sipple, and J. Peddle, "Objective load rating of a steel-girder bridge using structural modeling and health monitoring," *Journal of Structural Engineering*, vol. 139, no. 10, pp. 1771–1779, 2013.

[45] J. E. Phelps, "Instrumentation, Nondestructive Testing, and Finite Element Model Updating for Bridge Evaluation," Doctoral dissertation, Tufts University, Medford, MA, USA, 2010.

[46] M. Sanayei, A. J. Reiff, B. R. Brenner, and G. R. Imbaro, "Load rating of a fully instrumented bridge: Comparison of LRFR approaches," *Journal of Performance of Constructed Facilities*, vol. 30, no. 2, Article ID 04015019, 2016.